

To appear in the *Journal of Geophysical Research (Oceans)*, 1996.

Interdecadal variability and oceanic thermohaline adjustment

Richard J. Greatbatch and K. Andrew Peterson ^{1 2}

Department of Physics and Physical Oceanography, Memorial University of Newfoundland, St. John's, Newfoundland, Canada

Abstract

Changes in the strength of the thermohaline overturning circulation are associated, by geostrophy, with changes in the east-west pressure difference across an ocean basin. The tropical-polar density contrast and the east-west pressure difference are connected by an adjustment process. In flat-bottomed ocean models the adjustment is associated with viscous, baroclinic Kelvin wave propagation. Weak-high latitude stratification leads to the adjustment having an interdecadal timescale. We reexamine model interdecadal oscillations in the context of the adjustment process, for both constant flux and mixed surface boundary conditions. Under constant surface flux, interdecadal oscillations are associated with the passage of a viscous Kelvin wave around the model domain. We carry out experiments suppressing wave propagation along each of the model boundaries. Suppressing wave propagation along either the tropical or eastern boundary does not eliminate the oscillation, but increases both its period and amplitude. Suppressing wave propagation along either the polar or the western boundary eliminates the oscillation. Our results suggest the oscillations can be self-sustained by perturbations to the western boundary current arising from the southward boundary wave propagation. Mixed boundary condition oscillations are characterized by the eastward, cross-basin movement of salinity-dominated density anomalies, and the westward return of these anomalies along the northern boundary. We suggest the latter is associated with viscous Kelvin wave propagation. Under both types of boundary conditions, the strength of the thermohaline overturning and the tropical-polar density contrast vary out of phase. We show how the phase relationship is related to the boundary wave propagation. Box models and zonally averaged models assume that the east-west and north-south pressure gradients vary in phase and are proportional to one another. We suggest this assumption is valid only on timescales long compared to the adjustment timescale. The importance of boundary regions indicates an urgent need to examine the robustness of interdecadal variability in models as the resolution is increased, and as the representation of the coastal, shelf/slope wave guide is improved.

¹ Address: R.J. Greatbatch and K.A. Peterson, Department of Physics and Physical Oceanography, Memorial University of Newfoundland, St. John's, NF, Canada A1B 3X7 (email: rgreat@crosby.physics.mun.ca and drew@crosby.physics.mun.ca).

² This paper is also available from <ftp://crosby.physics.mun.ca/pub/drew/papers/gp1.ps.gz>

1. Introduction

Interdecadal variability is a fundamental feature of the climate system (see *Weaver and Hughes* [1992] for a review, and the recent papers by *Deser and Blackmon* [1993], *Kushnir* [1994], and *Latif and Barnett* [1994]). Interdecadal variability has also been found in coarse resolution (i.e., non-eddy resolving) ocean models. *Marotzke* [1990] and *Weaver and Sarachik* [1991] were the first to find such variability. These authors used mixed boundary conditions to represent the ocean/atmosphere interaction; that is, a strong (tens of days timescale) restoring boundary condition on the surface temperature and a constant flux boundary condition on the surface salinity. Interdecadal variability has also been found in models run under constant surface buoyancy flux [*Huang and Chou*, 1994; *Greatbatch and Zhang*, 1995; *Cai et al.*, 1995; *Chen and Ghil*, 1995] and in fully coupled ocean/atmosphere models [*Delworth et al.*, 1993; *Latif and Barnett*, 1994]. In addition, *Weaver et al.* [1994] have described an interdecadal oscillation in a coarse resolution North Atlantic model. *Greatbatch and Zhang* [1995] have noted the strong similarity between their oscillation under constant heat flux, and the oscillation found in the Geophysical Fluid Dynamics Laboratory (GFDL) coupled model [*Delworth et al.*, 1993]. *Griffies and Tziperman* [1995] have offered an alternative interpretation of the Delworth et al. oscillation using a four-box model run under mixed surface boundary conditions.

Central to interdecadal variability in ocean models are interdecadal fluctuations in the thermohaline circulation. The thermohaline circulation is driven by the formation of dense water in high latitudes in response to intense surface cooling. The new dense water spreads equatorward and is replaced at the surface by warm, salty water from lower latitudes. Consider a flat-bottomed ocean basin with both eastern and western boundaries. Assuming the north/south flow to be in geostrophic balance, then the northward transport per unit depth through a line of latitude ϕ and at depth z is given by

$$V(\phi, z) = \frac{(p_E - p_W)}{f\rho_0} \quad (1)$$

where p_E and p_W are the pressure on the eastern and western boundaries, ρ_0 is a representative density for seawater, and f is the Coriolis parameter. It follows that to understand fluctuations in the thermohaline overturning, it is necessary to understand what controls the east-west pressure difference across an ocean

basin. Undoubtedly, p_E and p_W will be strongly influenced by both coastal trapped wave propagation and advective processes in the boundary region (e.g., the Deep Western Boundary Undercurrent in the case of the North Atlantic). Equation (1) points to a fundamental issue in thermohaline ocean circulation theory, namely, that of how a north/south density gradient, established by high-latitude deep water formation, can set up the east/west pressure gradient necessary to maintain the geostrophic balance of the north/south flowing thermohaline circulation. *Zhang et al.* [1992] offer an explanation in terms of a “primary/secondary circulation” argument. The “primary circulation” is in thermal wind balance with the north/south density gradient, with eastward flow at the surface, and westward return flow beneath. The meridional boundaries block the primary circulation, leading to downwelling on the eastern boundary, and upwelling on the western boundary. This sets up east/west pressure gradients that then drive the north/south flow of the thermohaline circulation.

Zhang et al. [1992] did not discuss the details of the interaction between the primary circulation and the boundaries. In particular, they did not consider the role played by the coastal wave guide. In an early paper, *Davey* [1983] described the spin-up of a two-level model driven by a restoring surface boundary condition on temperature. The restoring temperature varied in the north/south direction. Davey noted that including meridional boundaries had a major impact on the spin-up, leading to an adjustment process involving coastal Kelvin waves and Rossby waves. *Wajsowicz and Gill* [1986] then went on to consider the spin-down of an ocean model initialized with a specified density field that varied only in the north-south direction. For their choice of initial density field, the first stage of the spin-down is accomplished by baroclinic, coastal Kelvin waves and takes place during the first few months of the model adjustment. *Wajsowicz and Gill* noted that these waves are severely corrupted by the coarse resolution and the large horizontal eddy viscosity commonly used in models [*Hsieh et al.*, 1983]. The second stage of the spin-down takes place on a decadal timescale and is associated with the propagation of long, baroclinic Rossby waves [*Wajsowicz*, 1986].

Recently, *Winton* [1996] has revisited the problem considered by *Wajsowicz and Gill* [1986]. Winton noted the importance of viscous boundary waves in models that exhibit interdecadal variability. The viscous boundary waves identified by Winton are the

low-frequency form of the viscous, baroclinic Kelvin waves noted by *Wajsbowicz and Gill* [1986]. At first sight, it may seem surprising that a Kelvin wave propagating along the boundary of a model domain could be important on an interdecadal timescale. If we consider a model extending from the equator to 60°N , and of 60° width in longitude, then a Kelvin wave propagating at 1 m s^{-1} (a typical speed for the first baroclinic mode) would take 0.7 years to travel the length of the boundary. Obviously, this timescale is considerably shorter than interdecadal. The key to the discrepancy rests with the model stratification, which is usually weak or nonexistent in the high latitudes owing to the presence of deep, convective mixing [Winton, 1996]. The weak stratification impedes wave propagation and leads to the emergence of an interdecadal timescale. *Wajsbowicz and Gill* [1986] did not notice this effect because the initial density stratification used in their spin-down experiment was not weak enough at high latitudes. The weak stratification can also lead to highly nonlinear behavior in the high latitudes and may be responsible for much of the sensitivity found in models [e.g., *Huang and Chou*, 1994].

Once it is appreciated that Kelvin wave adjustment in models has an interdecadal timescale, a question immediately arises as to the robustness of interdecadal variability in coarse-resolution ocean models. The inability to resolve the internal radius of deformation (especially in high latitudes where this is measurable in kilometers), the use of large eddy viscosity and diffusivity parameters, the inadequate representation of the ocean bottom topography, and the inadequate representation of boundary currents such as the Deep Western Boundary Undercurrent all preclude coarse-resolution models from resolving boundary processes as they occur in nature. A similar problem is the inability of models to adequately resolve the process by which North Atlantic Deep Water spills over the Greenland/Iceland/Scotland ridge and makes its way into the North Atlantic and the global ocean circulation [e.g., *Killworth*, 1992].

Recently, *Döscher et al.* [1994] have described the adjustment process in high-resolution eddy-resolving and non-eddy-resolving models of the North Atlantic. These authors considered the model response to a change in the temperature and salinity boundary condition applied along the northern boundary. They showed that the adjustment involves both wave and advective processes along the coastal and equatorial wave guides. They also showed that the adjustment

process depends on model resolution. In a related study, *Gerdas and Köberle* [1995] have examined the response of a $1^\circ \times 1^\circ$ model of the North Atlantic to a change in the surface temperature and salinity in the Denmark Strait region. Once again, the model shows a response in terms of both coastal trapped wave propagation and advective processes. In both these studies, the coastal trapped wave response is rapid, the waves excited in the northern North Atlantic reaching the equator on a timescale of weeks to months. This is followed by a much slower advective adjustment on a timescale of tens of years. These higher resolution studies suggest that the internal adjustment timescale of the ocean is indeed decadal, but they also suggest that in nature, advective processes may be more important than wave processes. On the other hand, neither of the problems studied in these papers involves wave propagation along a weakly stratified, high-latitude boundary.

A question fundamentally related to the adjustment process is that of the relationship between the strength of the thermohaline overturning circulation and the north/south density gradient. In box models [e.g., *Stommel*, 1961; *Griffies and Tziperman*, 1995] it is assumed that the former is directly proportional to the latter, with no phase lag. There is evidence, in models at least, that this relationship does not hold on interdecadal timescales. This is illustrated by Figure 1, taken from *Greatbatch and Zhang* [1995]. The figure shows anomalies (that is, difference from the mean) in the overturning stream function (left panels) and the zonally averaged temperature (right panels). The salinity is uniform, so that warmer/colder temperatures are associated with lighter/denser water. At the time in Figure 1b, the high latitudes are warmer, and therefore less dense, than in the mean, indicating a reduced density contrast between the equatorial and polar regions; yet, at this time, the overturning circulation in the basin reaches its maximum value. *Zhang et al.* [1995] describe a decadal oscillation in a coupled thermodynamic sea-ice/ocean circulation model that also shows some interesting phase relationships. In this case, the maximum in the overturning circulation is associated with the minimum in the convective overturning activity, and the minimum in the high-latitude surface heat loss.

In this paper, we reexamine interdecadal variability in ocean-only models. We begin with the thermal-only, constant surface flux oscillation of *Greatbatch and Zhang* [1995]. Since there is no variation in the surface forcing, oscillations under fixed surface flux

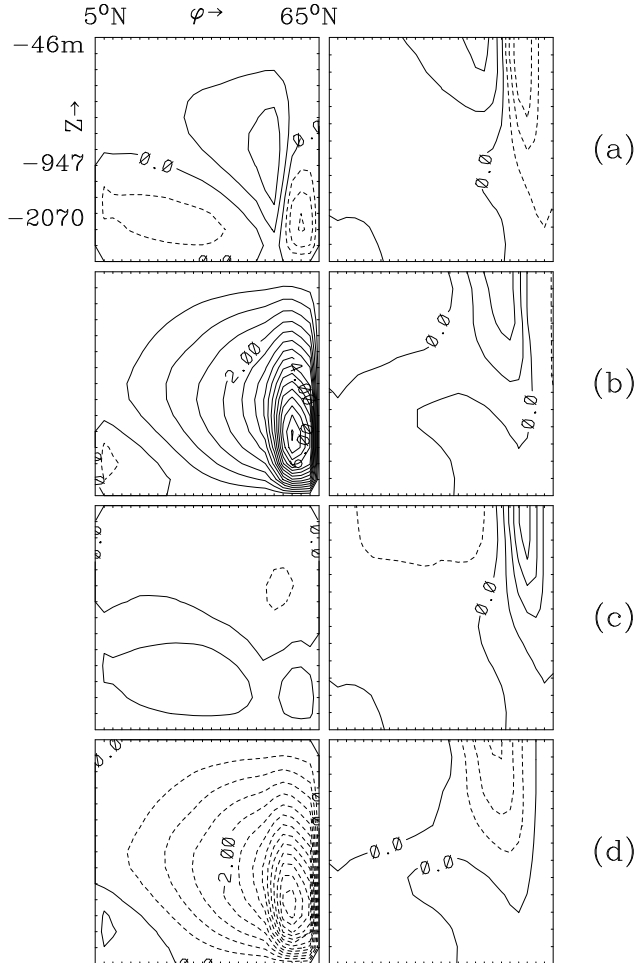


Figure 1. Anomalies (that is, difference from the mean) of the overturning stream function (left column) and the zonally averaged temperature (right column) taken from *Greatbatch and Zhang* [1995]. Figures 1a, 1b, 1c, and 1d are each 12.5 years apart, with the meridional overturning being a maximum at Figure 1b and a minimum at Figure 1d. The contour intervals are 0.5 Sv and 0.5°C, respectively. Negative anomalies are shown using dashed contours. The vertical scale is expanded in the upper part of the water column.

highlight the role of the internal adjustment process. We confirm *Winton's* [1996] conclusion that boundary waves play an important role in these oscillations. We explore the influence of wave propagation along each of the model boundaries and suggest a mechanism by which the oscillations can be self-sustained by perturbations to the western boundary current. We also discuss the phase relationship between the strength of the thermohaline overturning and the tropical-polar density contrast, and comment on the validity of parameterizations which assume these two quantities to be in phase and proportional. We also show that “zonal redistribution,” as discussed by *Cai et al.* [1995] is not always necessary for interdecadal oscillations to occur. In particular, we show results from a model run in which a self-sustained interdecadal oscillation occurs when the constant flux forcing is the same as the flux diagnosed from a spin-up experiment, all model parameters, model geometry, etc., being the same as in the spin-up. Finally, we reexamine decadal oscillations under mixed boundary conditions [e.g., *Weaver and Sarachik*, 1991]. The situation is now more complex because of the variable surface heat flux associated with the restoring boundary condition on the surface temperature. The role of boundary wave propagation along the model boundaries is demonstrated, and once again, we find that the strength of the thermohaline overturning and the tropical-polar density contrast vary out of phase with each other.

The structure of this paper is as follows. In section 2 we describe the model experiments. Section 3 gives the model results from cases run with thermal forcing only (uniform salinity). This section is divided into several parts: a small-amplitude oscillation, a large-amplitude oscillation, and the role of propagation along each of the model boundaries, where we also discuss how the oscillations are maintained. Section 4 discusses mixed boundary conditions, and section 5 provides a summary and discussion.

2. Model Description

We use a primitive equation, spherical coordinate model *Greatbatch et al.* [1995], very similar to the Bryan-Cox-Semtner model [*Bryan*, 1969; *Cox*, 1984; *Semtner*, 1974]. A realistic equation of state is used, like that of *Bryan and Cox* [1972]. The model domain is a flat-bottomed (4000 m depth) basin, extending from 5°N to 65°N, with a longitudinal extent of 60°. All the model experiments use the same 14 levels in

Table 1. The Depths of the Center of Each Model Level

Level	Depth, m
1	23.0
2	75.0
3	140.5
4	223.0
5	327.0
6	458.0
7	623.0
8	831.0
9	1093.0
10	1423.0
11	1838.5
12	2362.0
13	2990.5
14	3663.5

the vertical (the levels are given in Table 1), and have $2.4^\circ \times 2.4^\circ$ horizontal resolution. In addition, all experiments use uniform values of $10^{-3} \text{ m}^2 \text{ s}^{-1}$ and $10^{-4} \text{ m}^2 \text{ s}^{-1}$ for the vertical eddy viscosity and diffusivity, respectively, and are run with the wind forcing set to zero. Deep convection is parameterized as in the work by Cox [1984], by using a large value ($10^5 \text{ m}^2 \text{ s}^{-1}$) for the vertical diffusivity whenever a hydrostatically unstable density profile is generated. The model experiments are listed in Table 2 and differ in their surface forcing and model parameters.

We shall focus on two kinds of interdecadal variability found in ocean-only models, namely, the oscillations found under constant heat flux by *Greatbatch and Zhang* [1995] and oscillations found under mixed boundary conditions by *Weaver and Sarachik* [1991]. It follows that the model experiments are divided into two groups, as described below.

2.1. Temperature-Only Cases

In the temperature-only set of experiments (labeled A and B in Table 2) the model is run using a uniform value for the salinity of $35^\circ/\text{oo}$. There is no freshwater flux forcing.

First a restoring spin-up experiment is carried out, restoring the temperature in the top level of the model to a specified, zonally uniform restoring temperature

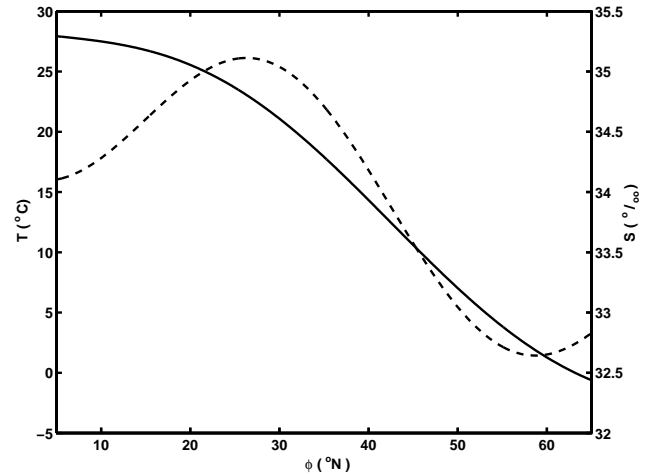


Figure 2. Zonal restoring temperature and salinity as a function of latitude. Solid line is temperature; dashed line is salinity.

given by

$$T_a(\phi) = 30.0 - 33.0/80.0 \times \phi + 4.0 \times \sin((2\pi/75.0)(\phi - 5.0)), \quad (2)$$

where ϕ is latitude in degrees (see Figure 2). The restoring timescale is 30 days. To increase the speed with which the model is brought to equilibrium, the acceleration techniques of *Bryan* [1984] are used. The acceleration is turned off for at least the last 500 years of the spin-up, and in all subsequent experiments. The exception is a mild distortion on the momentum equations (the local time derivative terms in the momentum equations are multiplied by a factor of 10). The latter allows the use of a longer time step than would otherwise be possible, and has no effect on the model results.

Following the spin-up, the surface heat flux into the ocean (in W m^{-2}) is diagnosed by calculating the average of Q_T , defined below, over the last 50 years of the spin-up. Q_T is given by

$$Q_T = \rho_0 c_p \gamma_T (T_a - T_1) \delta z, \quad (3)$$

where T_a is the restoring temperature given by equation (2), T_1 is the temperature in the top level of the model, γ_T is the restoring time constant ($1/\gamma_T = 30$ days), δz is the thickness of the top layer (46 m, and $\rho_0 c_p$ is density multiplied by specific heat at constant pressure. The diagnosed heat flux is then used to drive the model in subsequent experiments.

Table 2. The Model Experiments

Experiment	Horizontal Diffusivity, $\text{m}^2 \text{s}^{-1}$	Horizontal Viscosity, $10^3 \text{m}^2 \text{s}^{-1}$	Grid Size, deg	Surface Flux	Period, years	Maximum Amplitude, Sv	Mean Maximum, Sv
A0	2000	100.0	2.4	D	0.0	0.0	18.5
A1	2000	100.0	2.4	Z	33.9	2.6	15.0
B0	1000	100.0	2.4	D	30.5	7.7	17.3
B0a ^a	1000	100.0	2.4	D	37.2	11.5	19.9
B0b ^b	1000	100.0	2.4	D	36.2	10.3	20.6
B0c ^c	1000	100.0	2.4	D	0.0	0.0	18.3
B0d ^d	1000	100.0	2.4	D	0.0	0.0	18.2
C1	1000	100.0	2.4	RD	26-17	0.4-1.6	2.3-6.0

D, diagnosed flux; Z, zonal average of the diagnosed flux; R, restoring boundary condition. When two letters are used, the first refers to the heat flux, the second to the freshwater flux.

^aWave propagation suppressed on the southern boundary.

^bWave propagation suppressed on the eastern boundary.

^cWave propagation suppressed on the northern boundary.

^dWave propagation suppressed on the western boundary.

2.2. Temperature and Salinity Cases

In this set of experiments (labeled C in Table 2), the model is spun-up to equilibrium using restoring conditions applied to both the surface temperature and surface salinity. The restoring temperature is as before. The surface salinity is restored to a zonally uniform field (see Figure 2) given (in $^{\circ}/_{\text{oo}}$) by

$$S_a(\phi) = 35.0 - 1.32/50.0 \times \phi + 0.84 \times \sin((2\pi/55.0)(\phi - 15.0)). \quad (4)$$

A restoring timescale of 30 days is used, as for temperature. Upon reaching equilibrium, the corresponding surface heat and “virtual” salt fluxes are calculated (note that we use a virtual salt flux to drive the model, rather than the more realistic freshwater flux, as described by *Huang* [1993]). In analogy to equation (3), the surface salt flux is diagnosed from the last 50 years of the spin-up using

$$Q_S = \gamma_S(S_a - S_1)\delta z, \quad (5)$$

where S_a and S_1 are the restoring and top level model salinities respectively, γ_S is the restoring time constant ($1/\gamma_S = 1/\gamma_T = 30$ days), and Q_S is given in $^{\circ}/_{\text{oo}} \text{m s}^{-1}$.

2.3. Model Diagnostics

The most useful diagnostic is the baroclinic pressure defined by

$$P = p - \frac{1}{H} \int_{-H}^0 p dz \quad (6)$$

where

$$p = g \int_z^0 \{\rho - \bar{\rho}(z')\} dz' \quad (7)$$

$\bar{\rho}(z)$ is a reference density field that depends only on the vertical coordinate, z , and is usually taken to be the density averaged horizontally over the model domain and averaged in time over several oscillation periods. Since P is the baroclinic pressure, it has zero vertical average. It should be noted that because we do not include wind forcing, the barotropic flow in our model is very weak. As a consequence, the horizontal gradients of P are a very good approximation to the horizontal gradients of the total pressure.

3. Oscillations Under Constant Flux

3.1. A Small-Amplitude Oscillation

We begin with Experiment A0 in Table 2. The model is first spun-up, as described in section 2.

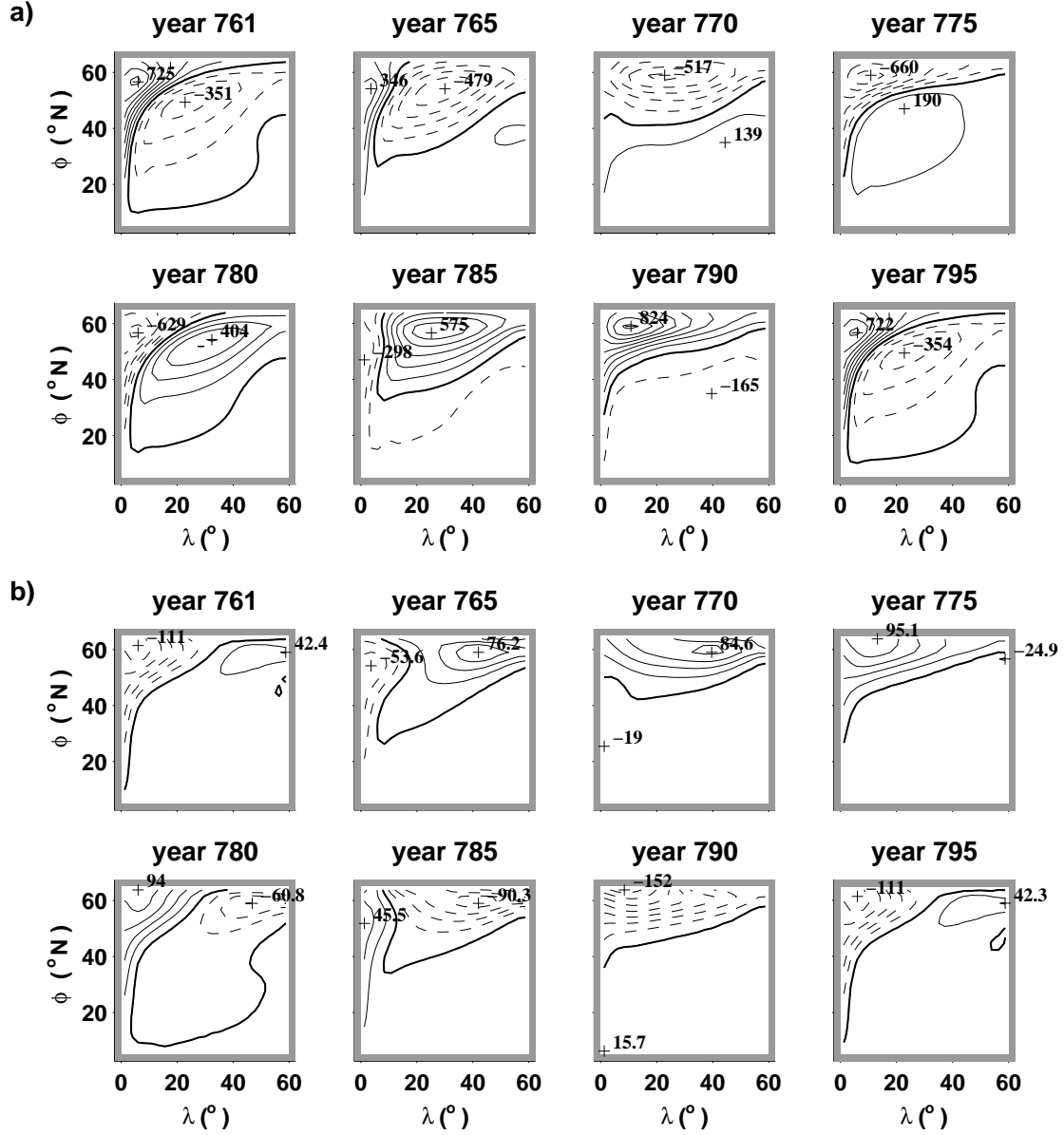


Figure 3. Experiment A1. Snapshots of baroclinic pressure anomalies (that is, difference from the mean averaged between years 612 and 984) for (a) level 1 (0 m to 46 m deep) with contour interval of 100 Pa and (b) level 12 (2070 m to 2654 m deep) with contour interval of 20 Pa. Negative values are shown using dashed contours. The maximum and minimum anomalies are displayed on contours (in Pa) and identified with a cross.

When the surface boundary condition is replaced by the diagnosed heat flux, and the model initialized with the end of the spin-up (all model parameters the same as in the spin-up), no oscillations are found; in particular, the model state remains unchanged. As discussed by *Cai et al.* [1995], oscillations can be induced by zonally redistributing the diagnosed flux (that is, replacing the diagnosed flux by a linear combination of the diagnosed flux and its zonal average). For simplicity, we restrict attention to the case in which the model is driven by the zonal average of the diagnosed flux (Experiment A1). Initializing with the end state of the spin-up, the model develops a steady oscillation with period 33.9 years. It should be noted that although we show results from model experiments that exhibit self-sustained oscillations, damped oscillations are also found if different model parameters and/or model resolution are used. Model results are particularly sensitive to the value of the horizontal diffusivity, an example of which is given in section 3.2 (examples of damped oscillations can also be found in the work by *Cai et al.* [1995]).

Figure 3 shows snapshots of the baroclinic pressure (defined by equation (6)) at the surface (Figure 3a) and at level 12 (Figure 3b; 2362-m depth) from Experiment A1. Anomalies in baroclinic pressure are plotted (that is, with the time average over many oscillations removed). Comparing the two depths, we see that the pressure anomalies are generally in phase but of opposite sign. Examination of the anomalies at other depths confirms the impression that the sign of the anomalies changes only once over the depth of the water column, indicative of the first baroclinic normal mode [*Gill*, 1982] (it should be noted that the depth of the zero crossing varies spatially, as one might expect, given the large spatial variations in the mean density field). The anomalous flow field associated with the anomalous pressure fields can be easily estimated from geostrophy. For example, at year 761, anomalous pressure is high at the surface on the western side of the model basin, and relatively low on the eastern side, implying anomalous southward flow at the surface and northward flow below (recall equation (1)). It is therefore not surprising to find that year 761 coincides with a minimum in the strength of the meridional overturning, whereas year 780, when the pressure pattern is reversed, is associated with a maximum in the overturning.

Associated with the anomalies in the strength of the overturning are strong gradients in anomalous baroclinic pressure along the model boundaries.

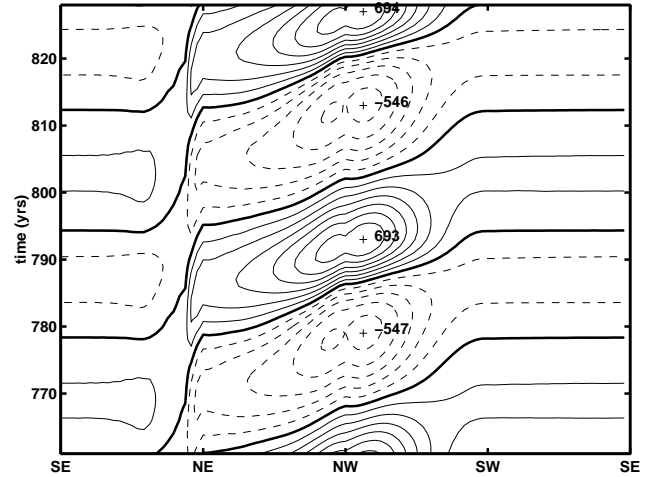


Figure 4. Experiment A1. Contours of baroclinic pressure anomaly at level 1 (surface) as a function of distance along the model boundary and time. Distance is measured in a counterclockwise direction from the southeast corner (marked SE). The contour interval is 100 Pa. Negative values are shown using dashed contours. The maximum and minimum values are displayed (in Pa) for each oscillation and identified with a cross.

For example, at year 761 (780), when the overturning strength is a minimum (maximum), there is an anomalous east-west pressure gradient along the northern boundary, with surface geostrophic flow away from (toward) the boundary. Geostrophic flow normal to the model boundary is associated with propagation along the boundary, as has been discussed by *Winton* [1996]. For example, when surface flow is toward the northern boundary, as at year 780, heat is advected toward the boundary. The convergence at the boundary warms the water column, raising the baroclinic pressure at the surface, and lowering it below. Since the flow is associated with high baroclinic pressure to the east, and low baroclinic pressure to the west, the result is a westward propagation of the pressure gradient associated with the flow. Propagation is clearly evident in Figure 4. The figure plots anomalous baroclinic pressure at the surface as a function of distance along the model boundary (abscissa) and time (ordinate). Distance along the boundary is measured counterclockwise from the southeast corner, labeled SE in the plot; the northeast, northwest, southwest, and southeast corners are labeled NE, NW, SW, SE, respectively. Clearly, the

interdecadal oscillation is associated with a disturbance that propagates along the model boundary, counterclockwise around the basin. Most of the oscillation period is spent propagating along the weakly stratified northern boundary, and the northern parts of the eastern and western boundaries. Propagation along the southern, and most of the eastern boundary, is much more rapid. Clearly, in the case shown, the disturbance propagates all around the model boundary in one oscillation period. In section 3.3, we shall address whether or not the disturbance must propagate all around the model domain in order to maintain the oscillation.

It might be thought that the propagating disturbance evident in Figure 4 is associated with advection by the mean flow. This is not the case, as can easily be understood by noting that the mean flow is toward the east throughout the upper part of the water column north of 50°N , but is toward the west beneath. This is not consistent with the propagation along the northern boundary, which is westward and almost in phase throughout the whole depth of the water column.

Following *Wajsovich and Gill* [1986], and the analysis given by *Winton* [1996], we interpret the boundary propagating disturbance as a coarsely resolved, viscous, baroclinic Kelvin wave. *Davey et al.* [1983] discuss the properties of these waves in a continuous medium, and *Hsieh et al.* [1983] discuss the modifications when these waves propagate on a finite difference grid, as in a numerical model. The low-frequency form of these waves described by *Winton* [1996] uses the Laplacian mixing term in the momentum equations to break the geostrophic balance, in order to allow divergence, and the associated vertical velocity, necessary for wave propagation. This contrasts with inviscid coastal Kelvin waves [*Gill*, 1982] for which the local time derivative terms are used to break geostrophic balance and allow vertical motion. It should also be noted that whereas the velocity normal to the coast is zero for an inviscid wave, this is not the case for waves with viscosity. *Winton* [1996] has noted that when the model resolution is insufficient to resolve the boundary layer, the waves take the form of the numerical boundary waves discussed by *Killworth* [1985]. Geostrophic balance is then broken by using the no-normal flow condition at the coast in the numerical computation of the divergence. An example is provided by the oscillation of *Greatbatch and Zhang* [1995]. These authors used the planetary geostrophic model of *Zhang et al.* [1992], which in-

cludes explicit friction only in the vertically averaged part of the flow. In *Greatbatch and Zhang's* study, the vertically averaged flow is zero, and the momentum equations reduce to geostrophy. Implementation of the no-normal flow boundary condition breaks the geostrophic balance at the coast and allows propagation of the numerical boundary waves. It is the existence of these waves that is responsible for the oscillation in *Greatbatch and Zhang's* [1995] paper.

An interesting aspect of Figure 4 is the special character of the northeast corner (marked NE). The almost complete elimination of the density stratification along the northern boundary strongly arrests wave propagation and gives the impression of disturbances being “held up” in the northeast corner. In this respect, it is interesting to consider Experiment A0, which does not oscillate. In the steady state, there is a horizontal pressure gradient along the eastern boundary associated with the surface eastward jet. Westward propagation of this jet is suppressed by the surface forcing, as demonstrated by *Winton* [1996], who shows an example where the surface forcing is removed, and a boundary wave immediately starts propagating along the northern boundary. We believe perturbations to the balance in the northeast corner play a role in initiating the wave propagation associated with the oscillation, as we demonstrate in subsection 3.3. Once wave propagation is initiated, the slow propagation along the northern boundary leads to a considerable increase in the amplitude of the wave. The slow propagation is itself related to the very weak model stratification, and plays a role in setting the interdecadal timescale of the oscillation.

In box models [*Stommel*, 1961; *Griffies and Tziperman*, 1995], it is assumed that the strength of the thermohaline circulation and the north/south density contrast vary in phase and are proportional to one another. By contrast, a necessary consequence of the thermal wind relation is the association of an enhanced (reduced) east-west, rather than north-south, density contrast with enhanced (reduced) north-south flow of the thermohaline circulation. In fact, the strength of the thermohaline overturning and the north-south density contrast do not vary in phase in our model, as can be seen from Figure 5. The solid line shows the time series of the maximum of the overturning stream function over one particular period of the oscillation. The dashed line shows the corresponding temperature averaged over the northern part of the basin (north of 35°N), subtracted from the temperature averaged over the southern part of

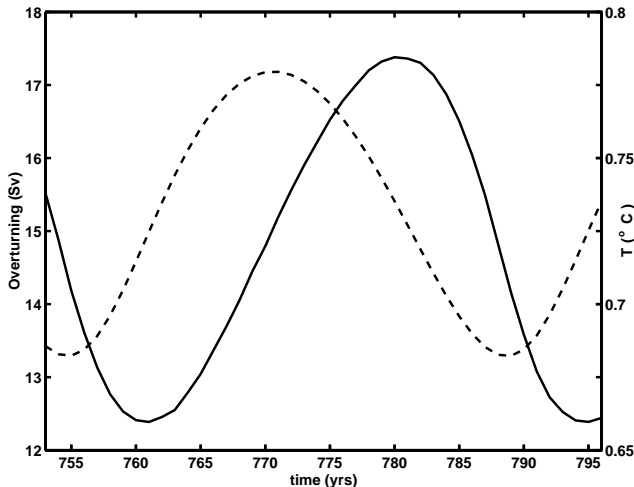


Figure 5. Experiment A1. Time series of the maximum in the overturning stream function (solid line), and the temperature averaged over the region north of 35°N subtracted from the temperature averaged over the region south of 35°N (dashed line).

the basin (south of 35°N). The choice of dividing latitude is not important; a similar result is obtained by using latitudes other than 35°N , including dividing latitudes that are close to the northern boundary. The north/south temperature difference is a measure of the north/south density contrast (recall that salinity is uniform in this experiment), with the maximum in the south/north temperature difference corresponding to the maximum in the north/south density difference. It is obvious that the maximum in the density contrast leads the maximum in the overturning by about 90° . This is not surprising in view of the previous discussion. In particular, the maximum in the overturning occurs at a time when the “east minus west” temperature difference, and associated baroclinic pressure gradient, reaches its peak along the northern boundary (a consequence of thermal wind). The maximum in this gradient is associated with the propagation of a warm front along the northern boundary, at which time the high latitudes are already warmer than in the mean.

The boundary adjustment process also has consequences for zonally averaged models. In these models, it is assumed that the east-west pressure difference is directly proportional to, and varies in phase with, the north-south pressure gradient [Wright and Stocker, 1991]. When the adjustment process is active, the as-

sumption breaks down, as illustrated by the pressure fields plotted in Figure 3. We suggest that the “in phase” relationship, assumed in box models and zonally averaged models, is valid only on timescales long compared to the adjustment timescale. For the flat-bottomed ocean models studied here, this timescale is decadal. Including variable bottom topography can alter the adjustment timescale because of the influence of variable bottom topography on the available wave modes, a topic of ongoing research. In a similar way, the adjustment timescale could be different in models of different resolution [Döscher *et al.*, 1994], with advective processes playing a more important role at high resolution, as in the study of Gerdes and Köberle [1995].

A question arises as to whether long, baroclinic Rossby waves play a role in the adjustment process in our model experiments. In the study of Wajsowicz and Gill [1986], these waves were important on the decadal timescale for spreading the influence of the eastern boundary into the ocean interior [Wajsowicz, 1986]. We have carried out many experiments using different model geometries in the hope of separating the Rossby wave effect from that of the boundary waves. These include basins with tilted eastern and western boundaries, and also experiments using the realistic coastline of the North Atlantic. In all cases, any influence of Rossby waves is secondary to the influence of the viscous Kelvin wave propagating around the boundary of the model domain. Indeed, it is always the latter that dominates the variation in the thermohaline overturning in the model experiments. The lack of an important role for Rossby waves is consistent with Winton [1996], who has showed that interdecadal variability is also found in models run on an f plane, for which there are no Rossby waves.

3.2. A Large-Amplitude Oscillation

Experiment B0 in Table 2 is spun-up exactly as Experiment A0, except that a smaller value ($1000 \text{ m}^2 \text{ s}^{-1}$) is used for the horizontal diffusivity. Following the spin-up, the surface boundary condition is switched to the diagnosed flux. Using the same model parameters as the spin-up, and initializing with the model state at the end of the spin-up, an oscillation of a 30.5-year period develops. This shows that zonal redistribution, as discussed by Cai *et al.* [1995], is not always necessary for the development of oscillations. It is also clear that the model behavior is sensitive to the value of the horizontal diffusivity, consistent with the sensitivity study of Huang and Chou [1994].

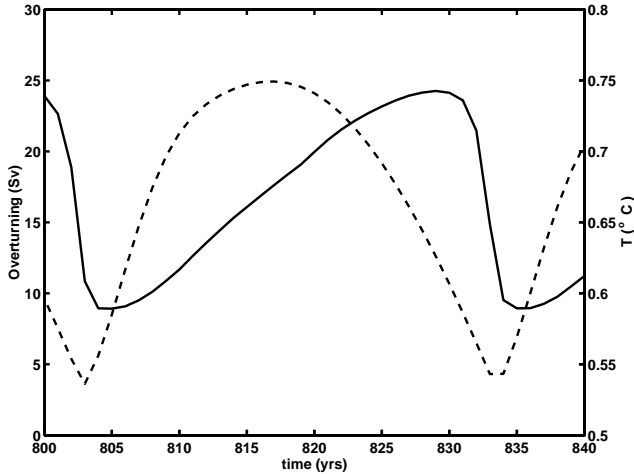


Figure 6. Experiment B0. Time series of the maximum in the overturning stream function (solid line), and the temperature averaged over the region north of 35°N subtracted from the temperature averaged over the region south of 35°N (dashed line).

The model variables in Experiment A1 undergo behavior that is close to being sinusoidal in nature (see Figure 5). In contrast, the oscillation that develops in Experiment B0 has a distinctly nonsinusoidal behavior, an indication of strong nonlinearity. As can be seen in Figure 6, there is now a strong asymmetry between the gradual strengthening phase of the oscillation and its sudden collapse. The stronger nonlinearity is also indicated by the much larger fraction of the mean overturning that is taken by the oscillation amplitude (roughly 0.45 in Experiment B0, compared to 0.17 in Experiment A1; see Table 2). As in Experiment A1, the strength of the overturning lags the north/south density contrast (see Figure 6), but the maximum in the overturning is now considerably delayed after the maximum in the north/south density contrast and, in fact, occurs only a few years before the minimum in that contrast.

As before, the oscillation is associated with the propagation of a wave around the model boundary (see Figure 7). The gradual strengthening of the overturning is associated with the slow propagation of a warm front along the northern boundary, the sudden collapse with the rapid movement of the front down the western boundary. Clearly, propagation of the warm front along the northern boundary (the strengthening phase) is quite different from propaga-

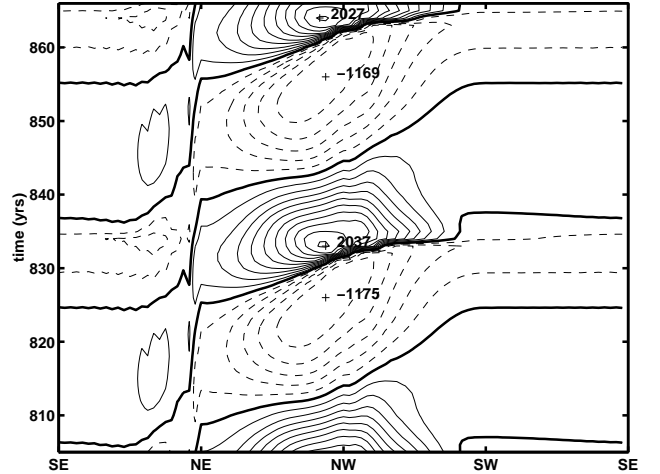


Figure 7. Experiment B0. Contours of baroclinic pressure anomaly (that is, difference from the mean averaged between the years 2586 to 2982) at level 1 (surface) as a function of distance along the model boundary and time. Distance is measured in a counterclockwise direction from the southeast corner (marked SE). The contour interval is 200 Pa. Negative values are shown using dashed contours. The maximum and minimum values are displayed (in Pa) for each oscillation and identified with a cross.

tion of a cold front. In Figure 7 the propagation of the warm front is associated with the steep gradient in baroclinic pressure that develops along the northern boundary around years 830 and 860. Close examination shows that ahead of the warm front, the water is mixed to the bottom, indicating no stratification. By contrast, behind the front, convective mixing occurs over only part of the water column. We believe it is the strong contrast in the density stratification either side of the front that gives the wave its highly nonlinear character. (There is an analogy here with a tidal river bore associated with an incoming tide.) In particular, points behind the wave front have increased stratification and therefore increased (local) gravity wave speed, compared to points ahead of the front, resulting in a steepening of the wave front.

3.3. The Role of Wave Propagation Along Each Model Boundary

The oscillation in both Experiments A1 and B0 is associated with the passage of a boundary wave once around the model domain (see Figures 4 and 7). The

question arises as to whether the wave must make a complete circuit of the boundary, and what role is played by the boundaries in maintaining the oscillations. For example, *Winton* [1996] has suggested that the oscillations are a consequence of thermal wind currents impinging on coasts with weak stratification. He points, in particular, to the surface eastward jet in the northern part of the basin impinging on the eastern boundary as being the source of decadal variability in models that oscillate under constant surface flux boundary conditions. To address these issues, we have carried out four experiments in which the wave propagation is suppressed along each of the southern, eastern, northern, and western boundaries. These experiments are labeled Experiments B0a,b,c,d, respectively, in Table 2. In the case of the southern boundary (Experiment B0a in Table 2), the experiment is identical to Experiment B0, except that along the four rows of grid points nearest the southern boundary, the temperature field is relaxed back to its initial value (that is, the state at the end of the spin-up). The timescale for this relaxation is 1.5 days nearest the boundary and 6.7 days along the outermost row of grid points. In the case of the other boundaries, the temperature field is relaxed back to its initial value only along the two rows of grid points nearest the boundary, the timescale for the relaxation being 2.5 days.

We begin with Experiment B0a, in which wave propagation is suppressed along the southern boundary. We find that an oscillation still occurs. The character of the oscillation is very much like that in Experiment B0, except that the amplitude is increased, and the period is now 37.2 years instead of 30.5 years. The fact that the period and amplitude are increased shows that allowing the wave to make a complete circuit of the model domain does have an effect, but it is not crucial for the existence of the oscillation. It is, nonetheless, of interest that preventing wave propagation along the remote, tropical boundary of the model domain does have an influence on high-latitude variability in the model.

When wave propagation is suppressed along the northern boundary (Experiment B0c), there is no oscillation, as we expect. The interesting experiments are B0b and B0d. In the former, wave propagation is suppressed along the eastern boundary. The oscillation still occurs and has a period of 36.2 years and amplitude of 10.3 Sv, both of which are similar to the period and amplitude in the case with wave propagation suppressed along the southern boundary. In

B0d, wave propagation is suppressed along the western boundary. This time no oscillation is found, a result that is surprising in view of *Winton's* [1996] suggestion that the oscillations are maintained by the eastward flowing jet impinging on the eastern boundary. If the oscillations were being generated on the eastern boundary, we should expect to see a wave propagating along the northern boundary from its eastern end, even though the wave propagation is being suppressed on the western boundary. It is also interesting that the oscillation is still found in Experiment B0b, even though the temperature field is being maintained at a constant value along the eastern boundary. We conclude that it is the western boundary that is the most important for maintaining the oscillation.

Propagation of the wave southward along the western boundary perturbs the western boundary current. We suggest that the perturbed western boundary current generates an anomaly in temperature that is then advected across the basin and initiates the wave propagation at the northeast corner. For example, at year 775 in Figure 3a, a surface low-pressure anomaly is propagating southwards down the western boundary. The northward intensification of the western boundary current leads to the warm, high-surface pressure, anomaly to the south, which in turn, links to the eastern boundary as the warm front associated with the strengthening phase of the oscillation starts propagating along the northern boundary. The special character of the northeast corner was noted in subsection 3.1, where we commented that in a steady state, the surface forcing must exactly balance the tendency for wave propagation along the northern boundary. It follows that a disturbance to this balance can lead to propagation. Amplification of the disturbance then takes place as the wave makes its way slowly along the weakly stratified northern boundary. In this way, we see the link to *Winton's* original suggestion that it is the eastern boundary that is important. In the case with propagation suppressed along the eastern boundary, the wave starts to develop from a point on the northern boundary just east of the northeast corner, which is consistent with the above idea. Allowing the wave to propagate from the western boundary, along the southern boundary and on up the eastern boundary, as in Experiment B0, adds an additional perturbation to the northeast corner region, allowing the northern boundary propagation to start slightly earlier. This effect is demonstrated by comparison with Experiments B0a and B0b, in which the propagation

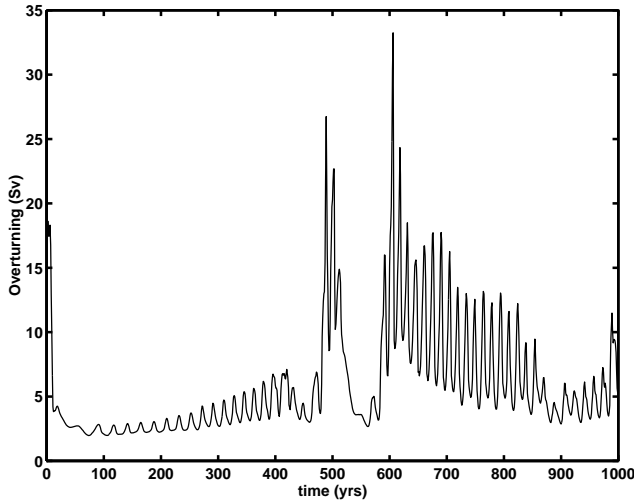


Figure 8. Experiment C1. Time series of the maximum in the overturning stream function in the case run under mixed surface boundary conditions.

is suppressed on the southern and eastern boundaries. Both Experiments B0a and B0b give oscillations of similar period and amplitude but with a longer period than in Experiment B0. It is also interesting to note that the above interpretation shows the relationship between oscillations under constant flux, and oscillations under mixed surface boundary conditions to be discussed next. In the latter, eastward movement across the basin interior is a pronounced feature of the oscillation. *Weaver and Sarachik* [1991] have associated this eastward movement with an advective process.

4. Mixed Boundary Conditions

We now consider what happens on a switch to mixed boundary conditions (Experiment C1 in Table 2). In other words, at the end of the spin-up, the surface boundary condition on salinity is replaced by the diagnosed flux, but the restoring boundary condition is maintained on temperature. Figure 8 shows a time series of the maximum in the overturning stream function. Upon the switch of boundary conditions, the circulation undergoes a rapid collapse (a polar halocline catastrophe; [Bryan, 1986]). After roughly 500 years, there is a flush, followed by subsequent collapses and flushes. Leading up to the first flush, there is a slow recovery of the overturning circulation, with decadal oscillations superposed. These oscilla-

tions have the same character as those discussed by *Weaver and Sarachik* [1991], as can easily be verified, and have a period that decreases from 26 years initially, to about 17 years. The oscillations are associated with large changes in the surface heat flux. The changes in surface heat flux act to keep the surface temperature close to the restoring temperature given by equation (2), as required by the restoring boundary condition. As such, oscillations under mixed boundary conditions are associated with surface buoyancy flux forcing that varies interdecadally, in contrast to the oscillations discussed in section 3, for which the surface buoyancy flux is constant in time.

As before, the baroclinic pressure proves to be a useful diagnostic. Figure 9 shows snapshots of the baroclinic pressure (the time mean has not been removed) at the surface and at level 11 (1838.5-m depth). The large features in midbasin are associated with salinity-dominated density anomalies that dominate the northern part of the basin, move eastward across the basin at midlatitudes, and then westward along the northern boundary (compare Figure 9 with Figure 10b). In midbasin, where the amplitude is large, the vertical structure of these features is like that of the first baroclinic mode, an indication of which is the different sign of the pressure anomalies at level 11 compared to the surface. Along the boundaries, the vertical structure is more complex, sometimes showing structure like that of higher baroclinic modes. Evidence of this is the multicell structure of the thermohaline overturning plotted in Figure 10a. Figure 11 plots the anomaly in the baroclinic pressure as a function of distance around the model boundary (as in Figure 4) at both the surface and at level 11 (1838.5-m depth). Once again, we see propagation in a counterclockwise direction around the model domain. This is particularly evident at level 11, where the oscillation is associated with the propagation of a disturbance all around the model domain, including the southern boundary (it should be noted that the location of the zero contour in Figure 11b is complicated by trends in the model variables associated with the gradual build up to the flush). Indeed, at depth, the characteristics of the oscillations under mixed boundary conditions have many similarities with those under constant surface flux boundary conditions.

We contend that viscous Kelvin wave propagation plays an important role in the westward movement of the anomalies across the northern boundary. We point first to the evidence of propagation along the boundary noted in the previous paragraph. The man-

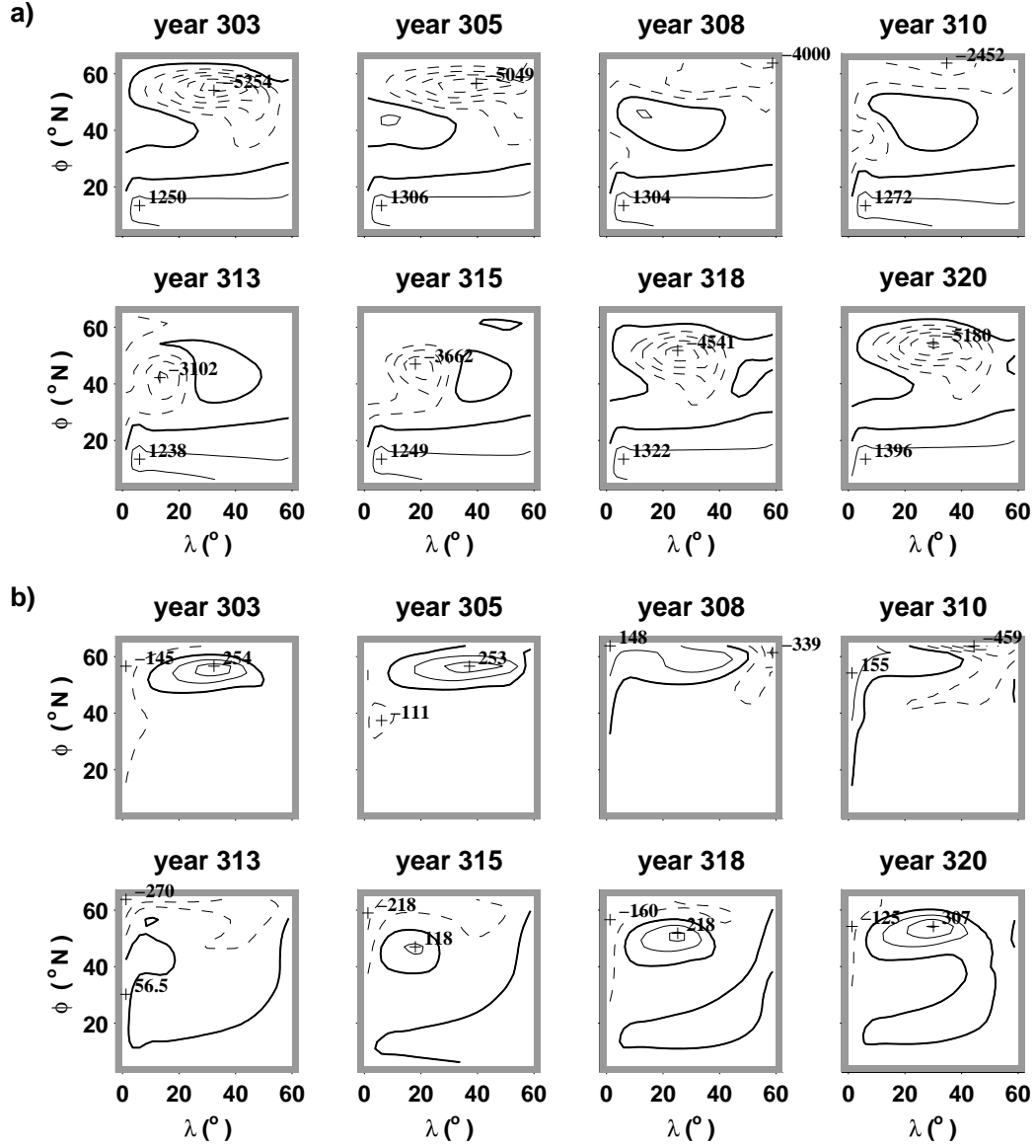


Figure 9. Experiment C1. Snapshots of total baroclinic pressure for (a) level 1 (0 m to 46 m deep) with contour interval of 1000 Pa and (b) level 11 (1607 m to 2070 m deep) with contour interval of 100 Pa. Negative values are shown using dashed contours. The maximum and minimum values are displayed on the contours (in Pa) and identified with a cross.

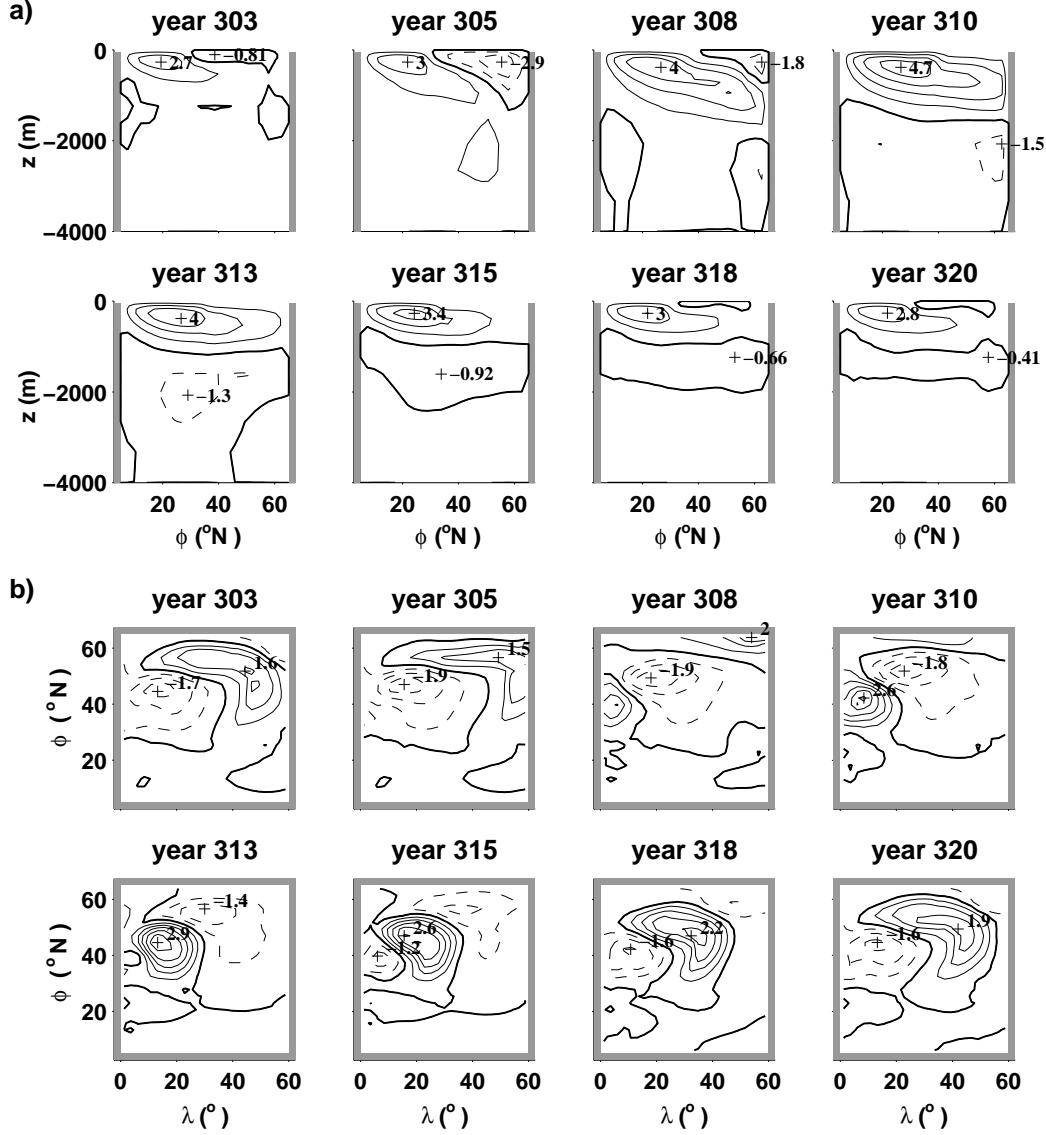


Figure 10. Experiment C1. Snapshots of (a) the overturning stream function with contour interval 1.0 Sv and (b) the surface salinity anomalies with contour interval $0.5^\circ/\text{oo}$. The meridional overturning has its minimum and maximum strength at years 303 and 310, respectively. Anomalies are differences from the mean state calculated by averaging from years 303 to 338. Negative values are shown using dashed contours. The maximum and minimum values are displayed on the contours (a) in Sv and (b) in $^\circ/\text{oo}$ and identified with a cross.

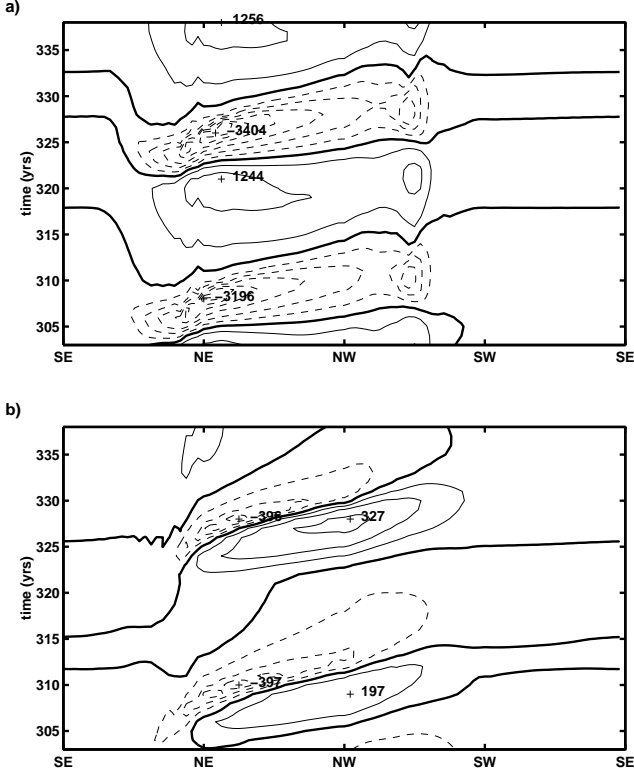


Figure 11. Experiment C1. Contours of baroclinic pressure anomaly as a function of distance along the model boundary and time at (a) level 1 (0 m to 46 m deep), with contour interval 500 Pa, and (b) level 11 (1607 m to 2070 m deep), with contour interval 100 Pa. Distance is measured in a counterclockwise direction from the southeast corner (marked SE). Negative values are shown using dashed contours. The maximum and minimum values are displayed (in Pa) for each oscillation and identified with a cross.

ner and characteristics of the propagation are consistent with the viscous Kelvin wave propagation noted in section 3. Furthermore, the similarity at depth between the structure of the mixed boundary condition oscillations discussed here and the constant flux oscillations discussed in section 3 adds further weight to the argument, particularly since the deeper depths are more isolated from the influence of the changing surface heat flux associated with the restoring boundary condition. Also, given the predominantly geostrophic nature of the flow in the model, the pressure fields plotted in Figure 9 clearly indicate regions of convergence and divergence that propagate along the model boundaries, and are the signature of wave propagation. We suggest that the convergence/divergence at the boundary is associated with the vertical movement of the anomalies that forms part of the explanation for the oscillation put forward by *Weaver and Sarachik* [1991].

An interesting aspect of the midbasin, eastward propagating anomalies is the association of strong surface heat loss with the positive salinity anomalies. The regions of strong surface heat loss move eastward with the positive salinity anomalies. Freshwater input at high latitudes, associated with the surface freshwater flux boundary condition, is mixed downward by convective overturning due to surface heat loss. Reduced surface heat loss allows the freshwater to accumulate at the surface, leading to a negative salinity anomaly [Zhang *et al.*, 1993]. Similarly, strong surface heat loss is associated with strong vertical mixing, which in turn, mixes surface freshwater downward, leading to a positive salinity anomaly at the surface. Viewed in this way, the eastward moving salinity anomalies can be regarded as being forced by the surface heat flux anomalies (that is, this part of the oscillation can be regarded as the forced part), whereas the westward movement along the northern boundary, which we have associated with viscous Kelvin wave propagation, can be regarded as the internal, unforced part of the oscillation. Of course, this argument does not address why the midbasin anomalies in surface heat flux move eastward. To understand this, it is necessary to consider the combined ocean-atmosphere system implied by the mixed surface boundary conditions. Certainly, existence of a surface freshwater anomaly would lead to reduced surface heat loss over the anomaly by the same mechanism by which a polar halocline catastrophe occurs [Zhang *et al.*, 1993]. Similarly, a positive salinity anomaly is associated with enhanced surface

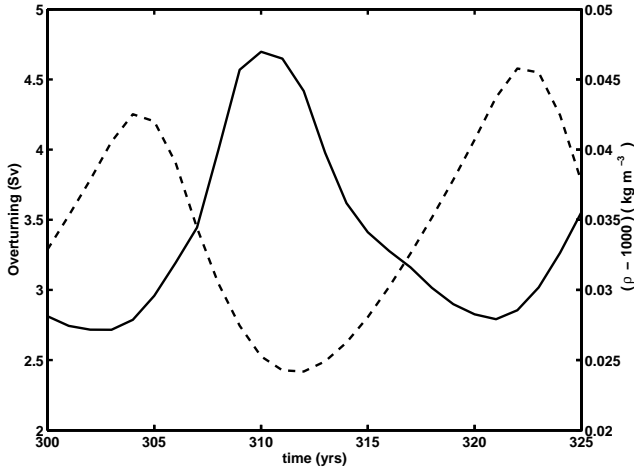


Figure 12. Experiment C1. Time series of the maximum in the overturning stream function (solid line), and the density averaged over the region north of 35°N subtracted from the density averaged over the region south of 35°N (dashed line).

heat loss at the surface, since the surface water is warmer due to deep convective mixing. We suspect the salinity anomalies are advected eastwards, as suggested by *Weaver and Sarachik* [1991] and carry the surface heat flux anomalies with them. However, because the anomalies completely dominate the total pressure field north of 30°N (see Figure 9), the details of the advective mechanism are not trivial, a point we shall return to in a later manuscript.

Figure 12 compares the strength of the overturning circulation with the north/south density contrast. Once again, we see that the two quantities do not vary in phase, the thermohaline overturning lagging the north-south density difference. Given the large anomalies that are found north of 35°N (Figure 9), it is not surprising that this time there is some dependence on the choice of dividing latitude used for the calculation. We feel, however, that the choice of 35°N is probably the most appropriate, since then the anomalies associated with the oscillation occur almost entirely north of the dividing latitude, the mean density south of the dividing latitude changing little during the oscillation. With this choice of dividing latitude, the thermohaline overturning lags the north-south density contrast by almost 180° .

We can understand the phase relationship by comparing Figure 12 with the baroclinic pressure fields

plotted in Figure 9. At years 303 and 305, the thermohaline overturning is at its minimum, and in fact, there is a shallow reverse cell north of 40°N (see Figure 10a). At this time, a large, positive density anomaly, associated with saline water, occupies the northern half of the basin (Figure 10b). This is associated with a large cyclonic eddy at the surface, with anticyclonic circulation at level 11 (Figure 9). The presence of the cyclonic eddy, and its associated positive density anomaly, explains why the north-south density contrast is enhanced, even though the thermohaline overturning is weak. It should also be noted that the deep convective mixing is strong, in association with the dense water of the cyclonic eddy, even though the thermohaline overturning is a minimum (this particular out-of-phase relationship is a feature of the ice-ocean oscillation of *Zhang et al.* [1995], which also uses mixed surface boundary conditions). The weak, surface-confined reverse cell of the thermohaline circulation is associated with the impingement of the cyclonic eddy on the eastern boundary, implying that the surface pressure is lower on the eastern than on the western boundary. It should be noted that most of the circulation associated with the cyclonic eddy makes no contribution to the thermohaline overturning, with the surface northward flow in the east being cancelled by surface southward flow in the west (it is the east-west pressure difference between the boundaries that matters). The increase in the strength of the thermohaline circulation is associated with the passage of a boundary wave along the weakly stratified part of the eastern boundary and the northern boundary. Pressure decreases at level 11 and increases at the surface with the passage of the wave, the surface lagging level 11 by several years. At year 310, the thermohaline overturning reaches its maximum. The northward surface flow toward the northern boundary, with southward flow away from the northern boundary at level 11, can be seen in Figure 9. At this time, a reduced density anomaly, associated with relatively fresh water, is present in the basin interior (Figure 10b) and explains the minimum in the north-south density contrast.

5. Summary and Conclusions

The oceanic thermohaline circulation transports roughly half the heat from low to high latitudes required to maintain the Earth’s radiation balance [*Gill*, 1982]. For the north-south flow to be in geostrophic balance, there must be an east-west pressure difference across the ocean basin. A fundamental ques-

tion is how the east-west pressure difference is established, given an initially imposed north-south density gradient. This problem has been studied by *Wajsowicz and Gill* [1986] and, more recently, by *Winton* [1996] and is closely related to the adjustment problem considered by *Davey* [1983]. In flat-bottomed ocean models the first stage of the adjustment is carried out by viscous baroclinic Kelvin waves [*Wajsowicz and Gill*, 1986]. The second stage involves internal Rossby waves *Wajsowicz* [1986]. *Wajsowicz and Gill* [1986], use a Kelvin wave adjustment timescale of only months, much less than the interdecadal timescale. On the other hand, the initial density field used by *Wajsowicz and Gill* [1986] had vertical density stratification at all latitudes, facilitating wave propagation all around the model domain. A feature of the models we have considered [see also *Winton*, 1996] is that the high-latitude density stratification is weak or nonexistent, greatly impeding internal Kelvin wave propagation. In fact, the presence of weak stratification, due to deep convective mixing, so impedes wave propagation that the adjustment by Kelvin waves now takes place on an interdecadal timescale. We have seen evidence of viscous Kelvin wave propagation in model experiments run under constant surface heat flux (salinity kept uniform and constant) and under mixed surface boundary conditions (a strong restoring boundary condition on the surface temperature, and a constant flux boundary condition on the surface salinity). We suggest that oscillations under constant surface flux are self-sustained by perturbations to the western boundary current arising from the southward propagating boundary wave along the western boundary. These perturbations are then advected to the northeast corner and play a role in reinitiating the wave propagation. Under mixed surface boundary conditions, salinity-dominated density anomalies move eastward across the interior of the basin and then westward along the northern boundary. We suggest the latter is associated with viscous Kelvin wave propagation. Under mixed surface boundary conditions, the westward advective phase is amplified by the changing surface heat flux in response to the surface salinity anomalies. Under constant surface flux, the amplification of the oscillation is associated with the wave propagation along the weakly stratified northern boundary.

We have not addressed the question of why oscillations are found under some surface flux fields but not under others [*Cai et al.*, 1995]. Experiment B0 is an example of an oscillation that occurs when the sur-

face restoring boundary condition used for the spin-up is replaced by the diagnosed surface flux, all other aspects of the model being the same as in the spin-up. On the other hand, Experiment A1 is an example where it was necessary to zonally redistribute the diagnosed flux to obtain oscillations. The two cases differ only in the value of the horizontal diffusivity (see Table 2). We suggest the horizontal diffusivity is an important parameter for determining whether self-sustained oscillations occur or not. The choice of horizontal diffusivity is, in turn, dependent on the model resolution and the choice of other mixing parameterizations, indicating that these choices can also influence the ability to obtain self-sustained oscillations in a model. Detailed discussion of this point is beyond the scope of the present paper.

Throughout this paper, we have argued that boundary wave propagation is essential for the existence of the variability we have described. This is very different from a situation in which variability is generated by a mechanism independent of boundary waves. In such a case, boundary waves could be excited as forced waves, but would then be symptoms of the variability, rather than essential to its existence. *Rahmstorf et al.* [1996] have drawn an instructive analogy between constant surface flux oscillations in three-dimensional models, and the thermal “loop” oscillator of *Welander* [1967]. The loop oscillator consists of the closed loop of fluid in the vertical plane, cooled at the top and heated at the bottom. A cold anomaly in the sinking branch will accelerate the flow. The anomaly then passes quickly through the heating region, but only slowly through the cooling region, maintaining the oscillation. The crucial ingredient is the time delay between the strength of the flow and the density contrast between the top and bottom of the loop. In the case of the loop oscillator, the time delay is provided by the fluid inertia. In three-dimensional ocean models, the time delay is provided by the boundary wave propagation associated with the thermohaline adjustment process, as indicated by the out of phase relationship between the strength of the overturning circulation and the tropical-polar density contrast (Figures 5, 6, and 12).

The out-of-phase relationship demonstrated in Figures 5, 6, and 12 stands in sharp contrast to the assumption in box models [*Stommel*, 1961; *Griffies and Tziperman*, 1995], that the thermohaline circulation and tropical-polar density contrast are in phase and proportional to one another. The adjustment process also invalidates the assumption in zonally-averaged

models that the east-west pressure difference is directly proportional to the north-south pressure gradient [Wright and Stocker, 1991]. We believe both assumptions are valid only on timescales long compared to the adjustment timescale. For the flat-bottomed ocean models we have considered, the adjustment timescale is clearly decadal. Including variable bottom topography may change the adjustment timescale because of the influence of the bottom topography on the available wave modes, and is a topic of ongoing research.

Although we have concentrated on the role of viscous baroclinic Kelvin waves, the studies by Döscher *et al.* [1994] and Gerdes and Köberle [1995] point to the importance of advection, rather than boundary waves, in setting the interdecadal timescale of the adjustment in higher resolution models (although the problems studied in these papers do not involve wave propagation along a weakly stratified, high-latitude boundary). In fact, it is clear that a major failing of coarse resolution models is the inadequate way in which they represent the coastal wave guide. This applies not only to the way in which wave processes are represented, but also to the representation of shelf/slope currents, such as the Labrador Current and the Deep Western Boundary Undercurrent. Given the importance of the wave guide demonstrated in this paper, and that of Winton [1996], it is clear that studies are required to test the robustness of interdecadal variability in models to both increasing resolution, and a more realistic representation of coastal, shelf/slope, processes. Recent data studies (G. Reverdin *et al.*, Decadal variability of hydrography in the upper northern North Atlantic 1948-1990, submitted to *Journal of Geophysical Research*, 1996) point to the importance of shelf/slope currents as a source region for interdecadal variability observed in the North Atlantic, again pointing to the need for more realistic representation of shelf/slope regions in models.

Acknowledgments Funding to R.J.G from NSERC, NSERC/WOCE, and AES in the form of a Science Subvention award, and a grant from the Canadian Institute for Climate Studies, are acknowledged. Comments from Stephen Griffies and two anonymous reviewers led to improvements in the manuscript.

References

- Bryan, K., A numerical method for the study of the circulation of the world ocean, *J. Comput. Phys.*, **4**, 347-376, 1969.
- Bryan, K., Accelerating the convergence to Equilibrium of Ocean climate model, *J. Phys. Oceanogr.*, **14**, 666-673, 1984.
- Bryan, F., Maintenance and variability of the thermohaline circulation, Ph.D. thesis, Program in Atmos. and Oceanic Sci., Princeton Univ., Princeton, N.J., 1986.
- Bryan, K., and M.D. Cox, An approximate equation of state for numerical models of the ocean circulation, *J. Phys. Oceanogr.*, **2**, 510-514, 1972.
- Cai, W., R.J. Greatbatch, and S. Zhang, Interdecadal variability in an ocean model driven by a small, zonal redistribution of the surface buoyancy flux, *J. Phys. Oceanogr.*, **25**(9), 1998-2010, 1995.
- Chen, F., and M. Ghil, Interdecadal variability of the thermohaline circulation and high-latitude surface fluxes, *J. Phys. Oceanogr.*, **25**(11), 2547-2568, 1995.
- Cox, M.D., A primitive equation, 3-dimensional model of the ocean, Tech. Rep. *1*, Geophys. Fluid Dyn. Lab. Ocean Group, GFDL/Princeton Univ., Princeton, N.J., 1984.
- Davey, M.K., A two-level model of a thermally forced ocean basin, *J. Phys. Oceanogr.*, **13**, 169-190, 1983.
- Davey, M.K., W.H. Hsieh, and R.C. Wajsbowicz, The free Kelvin wave with lateral and vertical viscosity, *J. Phys. Oceanogr.*, **13**, 2182-2191, 1983.
- Delworth, T., S. Manabe, and R.J. Stouffer, Interdecadal variations of the thermohaline circulation in a coupled ocean-atmosphere model, *J. Clim.*, **6**(11), 1993-2011, 1993.
- Deser, C., and M.L. Blackmon, Surface climate variations over the North Atlantic Ocean during winter: 1900-1989, *J. Clim.*, **6**(9), 1743-1753, 1993.
- Döscher, R., C. W. Böning, and P. Herrmann, Response of circulation and heat transport in the North Atlantic to changes in thermohaline forcing in northern latitudes: A model study, *J. Phys. Oceanogr.*, **24**(11), 2306-2320, 1994.
- Gerdes, R., and C. Köberle, On the influence of DSOW in a numerical model of the North Atlantic general circulation, *J. Phys. Oceanogr.*, **25**(11), 2624-2642, 1995.

- Gill, A.E., *Atmosphere-Ocean Dynamics*, 662 pp., Academic, San Diego, Calif., 1982.
- Greatbatch, R.J., and S. Zhang, An interdecadal oscillation in an idealised ocean basin forced by constant heat flux, *J. Clim.*, 8(1), 81-91, 1995.
- Greatbatch, R.J., G. Li, and S. Zhang, Hindcasting ocean climate variability using time-dependent surface data to drive a model: An idealised study, *J. Phys. Oceanogr.*, 25(11), 2715-2725, 1995.
- Griffies, S.M., and E. Tziperman, A linear thermohaline oscillator driven by stochastic atmospheric forcing, *J. Clim.*, 8(10), 2440-2453, 1995.
- Hsieh, W.H., M.K. Davey and R.C. Wajswowicz, The free Kelvin wave in finite-difference numerical models, *J. Phys. Oceanogr.*, 13, 1383-1397, 1983.
- Huang, R. X., Real freshwater flux as a natural boundary condition for the salinity balance and thermohaline circulation forced by evaporation and precipitation, *J. Phys. Oceanogr.*, 23(11), 2428-2446, 1993.
- Huang, R. X., and L. Chou, Parameter sensitivity study of the saline circulation, *Clim. Dyn.*, 9, 391-409, 1994.
- Killworth, P.D., A two-level wind and buoyancy driven thermocline model, *J. Phys. Oceanogr.*, 15(11), 1414-1432, 1985.
- Killworth, P.D., Flow properties in rotating, stratified hydraulics, *J. Phys. Oceanogr.*, 22, 997-1017, 1992.
- Kushnir, Y., Interdecadal variations in North Atlantic sea surface temperature and associated atmospheric conditions, *J. Clim.*, 7(1), 141-157, 1994.
- Latif, M., and T.P. Barnett, Causes of decadal climate variability over the North Pacific and North America, *Science*, 266, 634-637, 1994.
- Marotzke, J., Instabilities and multiple equilibria of the thermohaline circulation, Ph.D. thesis, *Ber. Inst. Meereskd. Kiel*, 194, 126 pp., 1990.
- Rahmstorf, S., J. Marotzke and J. Willebrand, Stability of the thermohaline circulation, *The Warm Water Sphere of the North Atlantic Ocean*, edited by W. Krauss, Borntraeger, Stuttgart, Germany, 1996.
- Semtner, A.J., An oceanic general circulation model with bottom topography, Numerical Simulation of Weather and Climate, Tech. Rep. 9, 99 pp., Dep. of Meteorol., Univ. of Calif., Los Angeles, 1974.
- Stommel, H., Thermohaline convection with two stable regimes of flow, *Tellus*, 13, 224-230, 1961.
- Wajswowicz, R.C., Adjustment of the ocean under buoyancy forces, Part II, The role of planetary waves, *J. Phys. Oceanogr.*, 16(12), 2115-2136, 1986.
- Wajswowicz, R.C., and A.E. Gill, Adjustment of the ocean under buoyancy forces, Part I, The role of Kelvin waves, *J. Phys. Oceanogr.*, 16(12), 2097-2114, 1986.
- Weaver, A.J., and T.M.C. Hughes, Stability and variability of the thermohaline circulation and its link to climate, Rep. 92-5, 56 pp., Cent. for Clim. and Global Change Res., McGill Univ., Montreal, Canada, 1992.
- Weaver, A.J., and E.S. Sarachik, Evidence for decadal variability in an ocean general circulation model: An advective mechanism, *Atmos. Ocean*, 29(2), 197-231, 1991.
- Weaver, A.J., S.M. Aura, and P.G. Myers, Interdecadal variability in a coarse resolution North Atlantic model, *J. Geophys. Res.*, 99, 12,423-12,441, 1994.
- Welander, P., On the oscillatory instability of a differentially heated fluid loop, *J. Fluid Mech.*, 29, 17-30, 1967.
- Winton, M., The role of horizontal boundaries in parameter sensitivity and decadal-scale variability of coarse-resolution ocean general circulation models, *J. Phys. Oceanogr.*, 26, 289-304, 1996.
- Wright, D.G., and T.F. Stocker, A zonally averaged ocean model for the thermohaline circulation, Part 1, Model development and flow dynamics, *J. Phys. Oceanogr.*, 21(12), 1713-1724, 1991.
- Zhang, S., C.A. Lin, and R.J. Greatbatch, A thermocline model for ocean climate studies, *J. Mar. Res.*, 50(1), 99-124, 1992.
- Zhang, S., R.J. Greatbatch, and C.A. Lin, A re-examination of the polar halocline catastrophe and implications for coupled ocean-atmosphere models, *J. Phys. Oceanogr.*, 23(2), 287-299, 1993.
- Zhang, S., C.A. Lin, and R.J. Greatbatch, A decadal oscillation due to the coupling between an ocean circulation model and a thermodynamic sea-ice model, *J. Mar. Res.*, 53, 79-106, 1995.